



저작자표시-비영리-변경금지 2.0 대한민국

이용자는 아래의 조건을 따르는 경우에 한하여 자유롭게

- 이 저작물을 복제, 배포, 전송, 전시, 공연 및 방송할 수 있습니다.

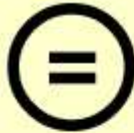
다음과 같은 조건을 따라야 합니다:



**저작자표시.** 귀하는 원저작자를 표시하여야 합니다.



**비영리.** 귀하는 이 저작물을 영리 목적으로 이용할 수 없습니다.



**변경금지.** 귀하는 이 저작물을 개작, 변형 또는 가공할 수 없습니다.

- 귀하는, 이 저작물의 재이용이나 배포의 경우, 이 저작물에 적용된 이용허락조건을 명확하게 나타내어야 합니다.
- 저작권자로부터 별도의 허가를 받으면 이러한 조건들은 적용되지 않습니다.

저작권법에 따른 이용자의 권리는 위의 내용에 의하여 영향을 받지 않습니다.

이것은 [이용허락규약\(Legal Code\)](#)을 이해하기 쉽게 요약한 것입니다.

[Disclaimer](#)

Thesis for the Degree of Master of Science

A new UHV system construction  
and the surface chemistry of  
 $D_2O$ /Zircaloy-4



by

Kyung-Sun Oh

Department of Chemistry  
The Graduate School  
Pukyong National University

August 2007

A new UHV system construction  
and the surface chemistry of  
D<sub>2</sub>O/Zircaloy-4

(새로운 UHV 시스템 제작과  
D<sub>2</sub>O/Zircaloy-4의 표면 화학)

Advisor : Prof. Yong-Cheol Kang

by

Kyung-Sun Oh

A thesis submitted in partial fulfillment of the requirements for the  
degree of

Master of Science

in Department of Chemistry, The Graduate School,  
Pukyong National University

August 2007

A new UHV system construction and the surface  
chemistry of D<sub>2</sub>O/Zircaloy-4

A Dissertation  
by  
Kyung-Sun Oh

Approved by :

\_\_\_\_\_  
(Chairman) : Dong J Lee

\_\_\_\_\_  
(Member) : Don Kim

\_\_\_\_\_  
(Member) : Yong-Cheol Kang

August 2007



3-1. The effect of Ar <sup>+</sup> sputtering by using XPS .....	20
3-2. The effect of annealing by using XPS .....	27
3-3. The UPS results after Ar <sup>+</sup> sputtering .....	33
IV. CONCLUSION .....	35
V. REFERENCES .....	36
VI. APPENDIX .....	39
PROCEDURE FOR ULTRAVIOLET PHOTOELECTRON SPECTROSCOPY	
KOREAN ABSTRACT .....	42
ACKNOWLEDGMENT .....	43

## LIST OF FIGURES

Figure 1.	Schematic diagram of the XPS process, showing photoionization of an atom by the ejection of a 1s electron.	2
Figure 2.	The schematic diagram of a TPD experiment (B is heating rate (K/s)).	5
Figure 3.	The $KL_1L_{2,3}$ Auger electron process.	8
Figure 4.	Schematic representation (front view) of the new ultra high vacuum system.	12
Figure 5.	Schematic representation (top view) of the new ultra high vacuum system.	13
Figure 6.	Schematic representation of the new gas handling system.	14
Figure 7.	Schematic representation of XPS system.	19
Figure 8.	XP spectra of the Zr 3d of $D_2O$ exposed Zircaloy-4 surfaces after different $Ar^+$ fluences.	22
Figure 9.	XP spectra of the O 1s of $D_2O$ exposed	23

Zircaloy-4 surfaces after different Ar<sup>+</sup> fluences.

- Figure 10. Deconvolution of measured Zr 3d spectra of the D<sub>2</sub>O exposed Zircaloy-4 after different Ar<sup>+</sup> fluences (a) Zr 3d ; 0.00 x 10<sup>16</sup> Ar<sup>+</sup>/cm<sup>2</sup> and (b) Zr 3d ; 12.4 x 10<sup>16</sup> Ar<sup>+</sup>/cm<sup>2</sup>. 24
- Figure 11. Deconvolution of measured O 1s spectra of the D<sub>2</sub>O exposed Zircaloy-4 after different Ar<sup>+</sup> fluences (a) O 1s ; 0.00 x 10<sup>16</sup> Ar<sup>+</sup>/cm<sup>2</sup> and (b) O 1s ; 12.4 x 10<sup>16</sup> Ar<sup>+</sup>/cm<sup>2</sup>. 25
- Figure 12. The relative ratios of the Zr 3d (a) and O 1s (b) peaks of the surface of D<sub>2</sub>O exposed Zircaloy-4 as a function of the Ar<sup>+</sup> fluence. 26
- Figure 13. XP spectra of the Zr 3d of D<sub>2</sub>O exposed Zircaloy-4 after stepwise annealing process. 28
- Figure 14. XP spectra of the O 1s of D<sub>2</sub>O exposed Zircaloy-4 after stepwise annealing process. 29
- Figure 15. Deconvolution of measured Zr 3d spectra of D<sub>2</sub>O exposed Zircaloy-4 after thermal treatment (a) Zr 3d ; 300 K (b) Zr 3d ; 787 K and (c) Zr 3d ; 30

913 K.

- Figure 16. Deconvolution of measured O 1s spectra of D<sub>2</sub>O exposed Zircaloy-4 after thermal treatment (a) O 1s ; 300 K (b) O 1s ; 787 K and (c) O 1s ; 913 K. 31
- Figure 17. The relative ratios of the Zr 3d (a) and O 1s (b) peaks of the surface of D<sub>2</sub>O exposed Zircaloy-4 as a function of annealing temperature. 32
- Figure 18. UP spectra of D<sub>2</sub>O exposed Zircaloy-4 after Ar-ion sputtering (a) survey scan and (b) high resolution UP spectra near Fermi level. 34

# A new UHV system construction and the surface chemistry of D<sub>2</sub>O/Zircaloy-4

Kyung-Sun Oh

Department of Chemistry, Graduate School,  
Pukyong National University

## Abstract

A new ultra-high vacuum (UHV) system was designed and constructed for the studies of Zircaloy-4 surface chemistry. Ultra-high vacuum was achieved by a roughing pump (RP), a turbomolecular pump (TMP), a titanium sublimation pump (TSP) and two ion pumps (IP). The UHV chamber was equipped with Auger electron spectroscopy (AES), low-energy electron diffraction (LEED), a quadruple mass spectrometer (QMS), a gas handling system for temperature programmed desorption (TPD) and an argon ion gun for sample cleaning.

The surface chemistry of D<sub>2</sub>O dosed Zircaloy-4 surface followed by Ar-ion bombardment and annealing was studied by means of X-ray photoelectron spectroscopy (XPS) and ultraviolet photoelectron spectroscopy (UPS). In XPS study, the effects of the Ar<sup>+</sup> bombardment and annealing were clearly observed. The Ar<sup>+</sup> sputtering led to the gradual depletion of oxygen on the surface region and the annealing caused to remove the oxygen on the surface of Zircaloy-4. The decrease of oxygen on the surface region resulted in the change of oxidation states of zirconium from zirconium oxides to metallic zirconium. UPS study showed the dominant peak at around 13 eV and the peak at around 9 eV decreased, but the peak of the metallic Zr 4d state at the Fermi level developed as the oxygen vanished after stepwise Ar<sup>+</sup> fluences.

# I . THEORY

## 1. X-ray Photoelectron Spectroscopy (XPS)

X-ray Photoelectron Spectroscopy (XPS) is an effective and widely used surface analysis technique, with which most ultra high vacuum (UHV) compatible samples can be studied. XPS was developed in the 1960s by K. Siegbahn and his research group at Uppsala University in Sweden [1] and is often referred to as Electron Spectroscopy for Chemical Analysis (ESCA).

In an XPS experiment, an specimen is irradiated by low energy X-rays in UHV. This causes photoionisation of the atoms at the surface of specimen. Photoelectrons are emitted from energy levels determined by the electronic structure of the atom as shown in Figure 1. This analysis technique examines the kinetic energies of these photoelectrons to examine their energy distribution. From the results of this analysis, it is possible to infer which elements are present on the specimen, what their chemical states are, and in what quantities they are present.

In principle, the X-rays cause photoelectrons of kinetic energy  $E_k$  to be emitted from the specimen, where  $E_k$  is related to the X-ray energy  $h\nu$  and electron binding energy  $E_b$  by the Einstein relation [2(a)]:

$$E_k = h\nu - E_b - \phi$$

where  $\phi$  is work function of the specimen in case sample is solid.

XPS is truly a surface analysis technique as only those photoelectrons with mean free paths of a few atomic layers are able to escape from the material.

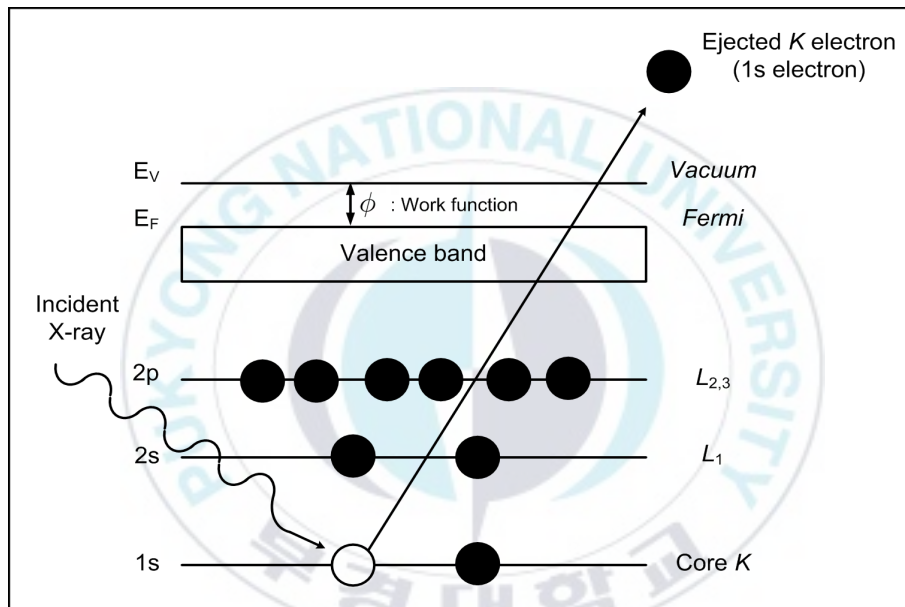


Figure 1. Schematic diagram of the XPS process, showing photoionization of an atom by the ejection of a 1s electron.

## **2. Ultra-violet Photoelectron Spectroscopy (UPS)**

Ultra-violet Photoelectron Spectroscopy (UPS) is ideally suited to providing information about the more weakly bound and less localised valence electronic states of surfaces. The low photon energies used result in high photoionisation cross sections and high energy resolutions. This makes UPS a valuable technique for studying the surface band structures of clean metals and ordered atomic adsorption layers on metals. Information about the nature of a molecule's interaction with a surface, such as bonding site, decomposition, orientation and interaction with other adsorbed species can be attained using this technique. The UPS technique is related to XPS but, whereas XPS is used for elemental identification by study of the strongly bound 'core' electrons, the domain of UPS is the study of the loosely bound valence levels that participate in chemical bond formation. The resulting photon energy is relatively low compared to XPS ( $< 50$  eV), and depend on the radiation used (He I, He II, Ne I etc.) and hence the UP spectra are confined to binding energies below the photon energies of these radiations [2(b)].

## **3. Temperature Programmed Desorption (TPD)**

Temperature programmed desorption (TPD) known as thermal desorption spectroscopy (TDS) is one of the earliest methods used in investigating the

state of adsorbates on surfaces. It involves heating a sample contained in vacuum and simultaneously detecting the residual gas in the vacuum by means of a mass analyser (quadruple mass spectrometer (QMS)) as shown in Figure 2. As the temperature rises, certain adsorbed species will have enough energy to escape and are able to desorb from the surface, then the pressure will rise. After that will be detected as a rise in pressure for a certain mass. If the temperature continuously rises, the amount of the adsorbed species on the surface will reduce and the pressure will drop again. This results in a peak in the pressure versus time plot.

The general rate expression for desorption process of the adsorbed species on the surface can be written as :

$$R_{des} = A \cdot N^x \exp \left( - E_a^{des} / R T \right)$$

where  $A$  is the pre-exponential (or frequency) factor,  $R_{des}$  is desorption rate ( $= -dN/dt$ ).  $x$  is the kinetic order of the desorption process (typically 0, 1 or 2) and  $E_a^{des}$  is activation energy for desorption. The values of  $A$  and  $x$  can be deduced and thus  $E_d$  can be calculated [3].

The area under a peak is proportional to the amount originally adsorbed, i.e. proportional to the surface coverage. The kinetics of desorption (obtained from the peak profile and the coverage dependence of the desorption characteristics) give information on the state of aggregation of the adsorbed species. The temperature of the peak maximum provides information on the binding energy

of the bound species. The position of the peak (the *peak maximum temperature*) is related to the enthalpy of adsorption, i.e. to the strength of binding to the surface.

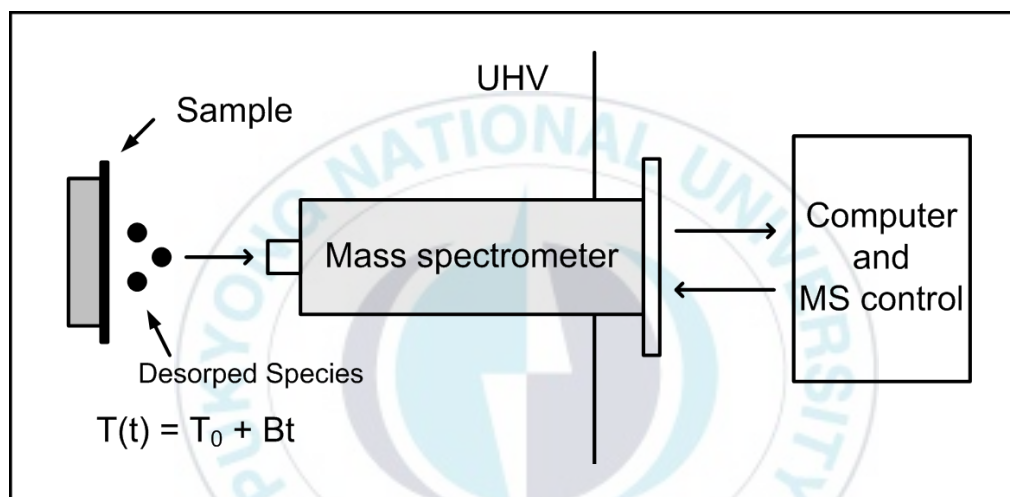


Figure 2. The schematic diagram of a TPD experiment (B is heating rate (K/s)).

#### **4. Auger Electron Spectroscopy (AES)**

Auger Electron Spectroscopy (AES) has developed to one of the most useful analytical techniques providing access to surface-chemical composition and, in many cases, the chemical state of the atoms in the surface region of a solid material. An Auger electron spectrum plots the number of electrons detected as a function of kinetic energy of electron. Elements are identified by the energy positions of the Auger peaks, while the concentration of an element is related to the intensity of its peaks. When combined with the necessary scanning electronics, AES can be used to map the distribution of elements in the surface with very high spatial resolution. Compositional depth profiles can be obtained by combining AES with ion beam sputter etching. Auger electron spectroscopy has found widespread use in an extensive variety of materials applications, especially those requiring surface specificity and high spatial resolution [4]. AES cannot detect hydrogen or helium, but is sensitive to all other elements, being one of the most sensitive techniques to the low atomic number elements.

The Auger process occurs after an atomic level has been ionized by incident photons or electrons. The hole in the inner shell is filled by one electron from a higher level and a secondary electron (called Auger electron) escapes into the vacuum with the remaining kinetic energy.

In the Figure 3, the first process is the ionization of an inner shell, say, a K shell (1s electron). The second process is the internal transition of an outer

electron, for example, and  $L_1$  electron (2s), to the K shell to fill the hole. Apparently, a second electronic level becomes involved here. The third process is the energy transfer to a third electron (the Auger electron), often of the same shell ( $L_2$  or  $L_3=2P_{1/2}, 2p_{3/2}$ ), but of course, also from an outer (M) shell. No matter from where the Auger electron is emitted, three electronic states participate in the process, and with relaxation phenomena neglected, the kinetic energy of the Auger electron can be written

$$E_{kin} = E_1 - E_2 - E_3 - \text{work function}$$

where  $E_1$  denotes the binding energy of the initial core electron prior to ionization,  $E_2$  that of the electron that fills the core hole, and  $E_3$  the binding energy of the ejected electron [5]. We call the process is  $KL_1L_{2,3}$ .

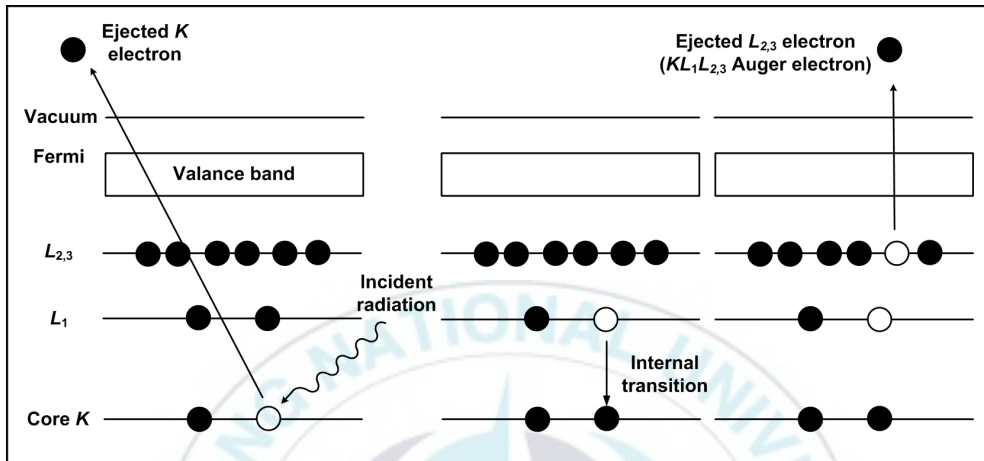


Figure 3. The  $KL_1L_{2,3}$  Auger electron process.

## **II. CHAPTER 1. Newly designed ultra-high vacuum (UHV) system**

All solid materials interact with the outside world by their surfaces. The surface chemistry will influence such factors as corrosion rates, catalytic activity, adhesive properties, contact potential, and failure mechanism. Surface, therefore, is important for the properties of the solids. In surface science, a vacuum system is used to produce a clean surface and maintain for a sufficiently long time for experimental investigations.

In this work, a new ultra-high vacuum (UHV) system was designed and constructed for the studies of Zircaloy-4 surface chemistry in our laboratory.

### **1. UHV chamber**

The vacuum chamber presented in Figure 4 (front view) and 5 (top view) was made of stainless steel (SUS 304) and consisted of a main chamber for surface analysis and a preparation chamber which was equipped with many pumps to get ultra high vacuum.

The pumping systems included a roughing pump (RP), a turbomolecular pump (TMP), a titanium sublimation pump (TSP) and two ion pumps. The RP and TMP were separated from the main chamber by gate valves. These pumps were used to evacuate the chamber from atmospheric pressure to high vacuum. One of the IPs and TSP were also separated by a main gate valve and the

other IP was directly equipped in the main chamber to maintain UHV condition.

The base pressure of this chamber was  $1 \times 10^{-10}$  torr as read with nude ion gauges. In this UHV chamber, two nude ion gauges were placed to measure the pressure in different regions of the system. One was placed on the analysis chamber and the other was attached on the preparation chamber.

The UHV chamber was equipped with a quadruple mass spectrometer (QMS) to display a local total pressure as the exposure of the gases from gas handling system for the temperature programmed desorption (TPD) experiment.

A 4-grid retarding field low-energy electron diffraction (LEED) system was combined with a Auger electron spectroscopy (AES) providing surface-chemical composition on the main chamber to determine surface structures. A digital camera will be used to record the back-scattered electron diffraction patterns appearing on a phosphor screen through a viewport.

Many view ports were also attached on the analysis chamber to see the position of samples and observe the specimens during the experiments.

An argon ion gun was located on the main chamber for sample surface cleaning.

## **2. Gas handling system**

A stainless steel gas handling system incorporating two precision variable leak valves is depicted in Figure 6. The custom-made gas handling system allowed

for controlled, reproducible and independent introduction of both inert and reactive gases into the main chamber.

The main chamber could be backfilled with the gas of interest. The gas line itself had two isolatable regions. One half of the system allowed the introduction of reactive gases and was monitored by a convectron gauge, while the other half of the gas line was for inert gas control.

### **3. Sample manipulator**

The vacuum chamber was also equipped with a manipulator that allowed limited sample motion along three orthogonal axes and provided rotational capability about the manipulator axis. The manipulator, denoted as the x, y, z, theta manipulator, allowed samples mounted on the manipulator arm to be cooled by liquid nitrogen as well as resistively heated and controlled by a temperature controller.

The sides of the samples, Zircaloy-4 and Pt<sub>3</sub>Co(100), were spot-welded to 0.5 mm diameter tantalum wires, which were in turn mounted onto machined copper arms. A copper braid connected a cold finger to one of the copper arms to provide cooling of the sample. Insulated wires were connected to the copper arms of the manipulator chassis for sample heating. The samples were electrically isolated from the manipulator arm by sapphire glass. Two type-K thermocouples were directly spot-welded onto the sides of the Zircaloy-4 and

Pt<sub>3</sub>Co single crystal to monitor sample temperature.

In the present, the surface chemistry of D<sub>2</sub>O/Zircaloy-4 is being studied using TPD and AES in the UHV system.

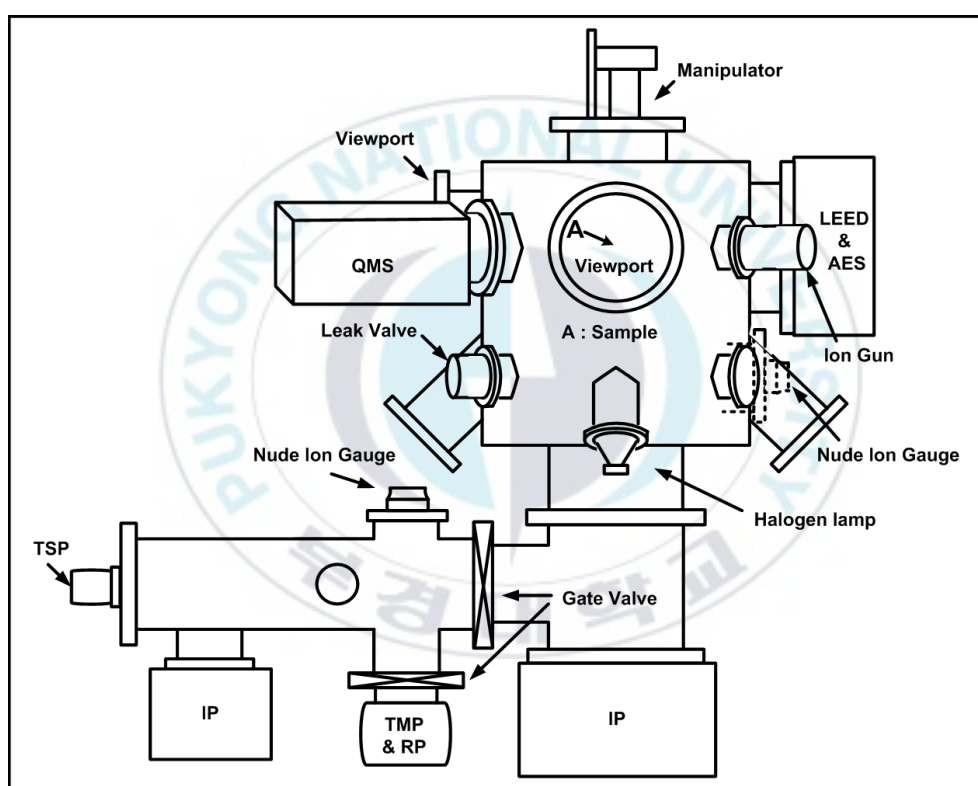


Figure 4. Schematic representation (front view) of the new ultra high vacuum system.

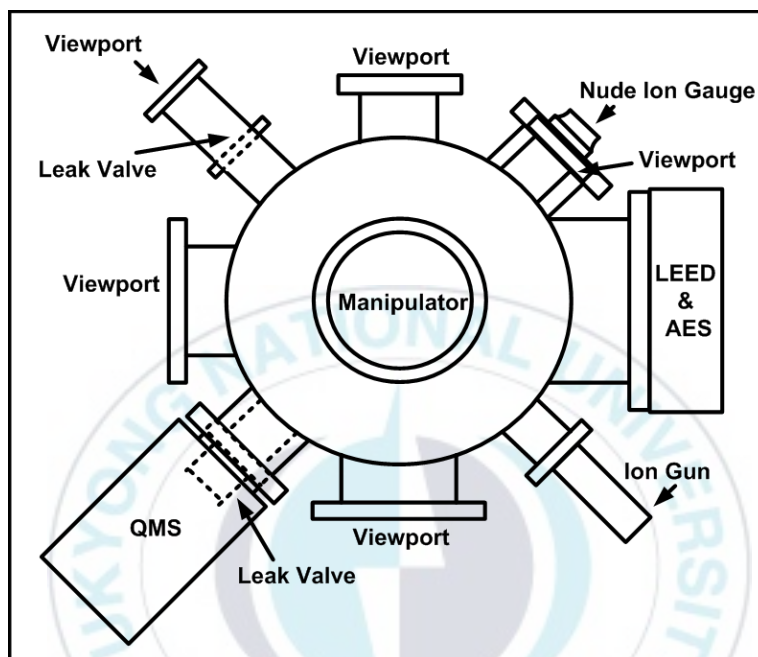


Figure 5. Schematic representation (top view) of the new ultra high vacuum system.

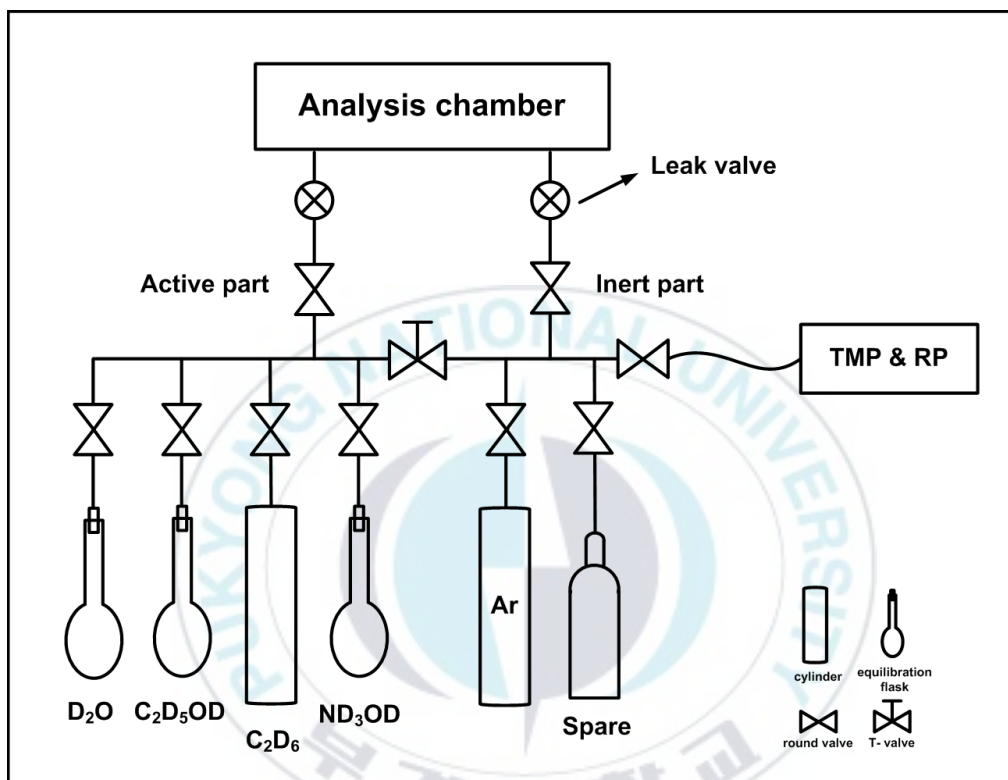


Figure 6. Schematic representation of the new gas handling system.

### **III. CHAPTER 2. The effects of Ar-ion bombardment and annealing of D<sub>2</sub>O/Zircaloy-4 surfaces using XPS and UPS**

#### **1. Introduction**

Zircaloy-4 is widely used in the nuclear industry as cladding materials for fuel containment in nuclear reactors, those are cooled by water/heavy water, because of its corrosion resistive property and low thermal neutron scattering cross-section. The corrosion [6-9], oxidation [10-13] or hydrogen absorption kinetics [14-17] of Zircaloy-4 and its nuclear applications have been of great concern and investigated with a variety of surface science techniques in the literatures. Zircaloy-4 oxidation by water (H<sub>2</sub>O) and steam environments has been reported in numerous studies [18-23]. The interaction of H<sub>2</sub>O with Zircaloy-4 was investigated using Auger electron spectroscopy (AES) and Temperature programmed desorption (TPD) methods by R.D. Ramsier et al [18]. They reported that following adsorption of H<sub>2</sub>O at 150 K, the Zr(MNV) and Zr(MNN) Auger features shifted by ~6.5 and 4.5 eV, respectively, indicating surface oxidation. Heating H<sub>2</sub>O/Zry-4 resulted in molecular desorption of water at both low and high temperatures. The effects of adsorbates on the oxidation of Zircaloy-4 in air and steam were studied by the measurement of the weight gain of specimens [19]. They reported that the effect of LiOH was dependent on the surface condition, temperature and the

type of atmosphere. The behavior of water with sulfur dioxide pre-exposed Zircaloy-4 surfaces was also studied in R.D. Ramsier's group [20]. They reported that adsorption of SO<sub>2</sub> caused shift of the Zr(MNN) Auger electron feature by 3.0 eV, whereas subsequent water adsorption attenuated the sulfur Auger signal and resulted in the development of a zirconium oxide, Zr(MNN), feature. However, despite the fact that a number of articles deal with the interaction of D<sub>2</sub>O on zirconium [24-25], little is known about the surface chemistry of deuterium containing species on Zircaloy-4 surfaces [26-27].

In this study, the effects of Ar-ion bombardment and annealing on the surface of D<sub>2</sub>O dosed Zircaloy-4 surface were investigated using XPS and UPS.

## **2. Experimental section**

### **2-1. Sample preparation**

Zircaloy-4 sample in this work had a surface area of 29.22 mm<sup>2</sup> from a sheet of Zircaloy-4. Its elemental composition is nominally 1.2~1.7 wt% Sn, 0.18~0.24 wt% Fe, 0.07~0.13 wt% Cr, 0.08~0.015 wt% O and the balance Zr [28]. The Zircaloy-4 sample was polished with abrasive papers and a mechanical polisher (Buehler, gamma alumina, 0.05 micron). After mechanical treatment, it was ultrasonically degreased in acetone for 20 min after dried with nitrogen gas. After ex situ D<sub>2</sub>O (99.999% purity, Aldrich) dosing on Zircaloy-4, the specimen was installed in an ultra high vacuum (UHV)

chamber.

## **2-2. UHV system**

The UHV chamber as shown in Figure 7 used in this study is pumped by two stages of pumping system and the pumping system is the same as the previous paper [29]. The first one is that a turbomolecular pump (TMP) backed by a two stage rotary vane pump (RP) system pumps a fast entry airload-lock (FEAL) chamber. And the second system consists of an ion getter pump and a Ti-sublimation pump and evacuates analysis chamber to maintain UHV condition. An ion sputtering gun is equipped in the analysis chamber for sample cleaning and depth profile study. A charge-coupled device (CCD) camera guides to set up the sample for X-ray and UV photoelectron analysis.

## **2-3. XPS and UPS experimental details**

The XPS and UPS experiments were carried out in UHV (base pressure  $7.5 \times 10^{-11}$  torr) chamber equipped with a concentric hemispherical analyzer (CHA), a twin anode X-ray source (Mg and Al  $K_{\alpha}$  1253.6 and 1486.6 eV, respectively) for XPS (VG ESCALAB 2000) and a UV source (He I 21.2 eV, He II 40.8 eV) for UPS.

During survey scans, XP spectra were obtained using Al  $K_{\alpha}$  x-ray source. X-ray source was at high voltage of 15 kV, beam current of 15 mA, filament current of 4.2 A, pass energy of 20 eV, dwell time of 50 ms and energy step size of 1 eV in constant analyzer energy (CAE) mode at large area XPS

(LAXPS) for annealing and small area XPS (SAXPS) for study of Ar-ion bombardment effect and other factors were same as the parameters used in the investigation of annealing effect. He I was used as the exciting source for UPS measurements. Pass energy of 2 eV, energy step size of 0.05 eV and large area UPS mode were applied for UPS survey scan and narrow scan. D<sub>2</sub>O dosed Zircaloy-4 sample was pre-pumped in the fast entry air loadlock (FEAL) chamber for approximately 2 hrs before loading into the analysis chamber which was pumped by a turbo molecular pump (TMP, 70 l/s) backed by a roughing pump (RP, 200 l/min). Obtained XPS Zr 3d and O 1s peaks were divided into several peaks according to their chemical environments by means of deconvolution process. The full width half maximum (FWHM) of each peak of Zr 3d and O 1s were between 1.3 and 2.5 eV, 1.5 and 2.3 eV, respectively, and G/L ratio of 27% (Lorentzian-27%, Gaussian-73%). Our XPS data were deconvoluted using XPSPEAK software (ver 4.1).

During Ar (99.999% purity, Aldrich) ion bombardment, the argon pressure was kept at  $7.5 \times 10^{-8}$  torr, the sample current was about 2.02  $\mu\text{A}$  and the argon fluence was  $0.52 \times 10^{16}$   $\text{Ar}^+/\text{cm}^2$  per 1 cycle of  $\text{Ar}^+$  sputtering. In the UPS measurements, the sample current was about 1.65  $\mu\text{A}$  and the argon fluence was  $0.39 \times 10^{16}$   $\text{Ar}^+/\text{cm}^2$  per 1 cycle of  $\text{Ar}^+$  sputtering.

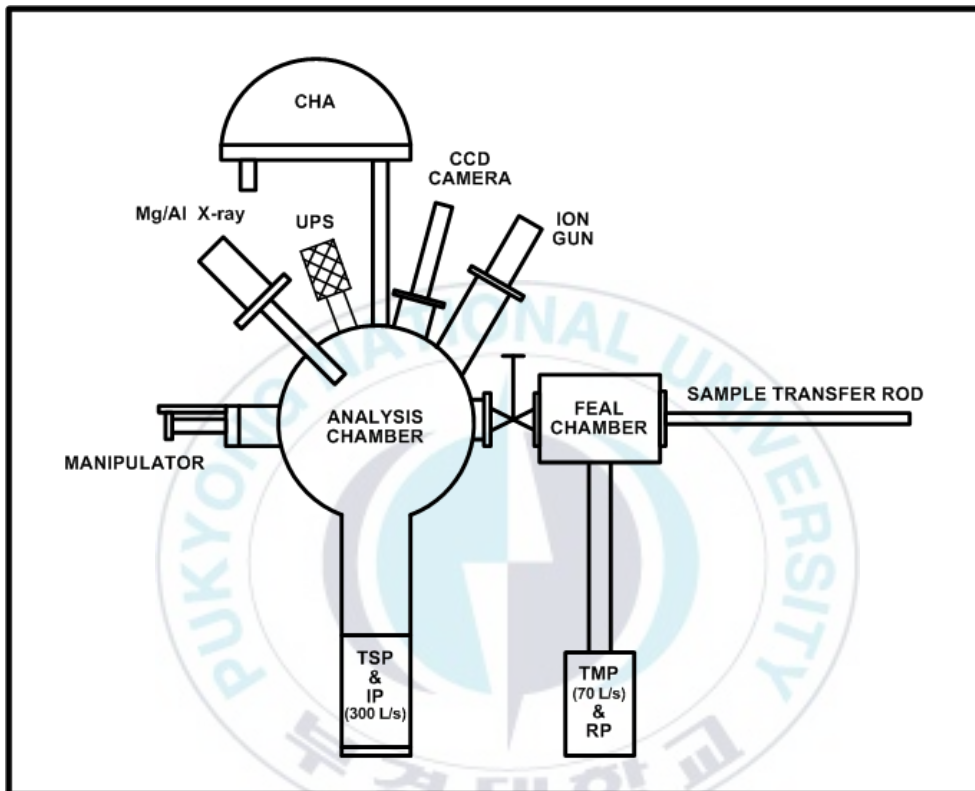


Figure 7. Schematic representation of XPS system.

### 3. Results and Discussion

#### 3-1. The effect of Ar<sup>+</sup> sputtering by using XPS

Figure 8 and 9 present the Zr 3d and O 1s XP spectra of D<sub>2</sub>O exposed Zircaloy-4 sample after different Ar<sup>+</sup> fluences (indicated in each spectrum). Prior to Ar<sup>+</sup> sputtering (bottom line in Figure 8), the XP spectra of Zr 3d showed four elementary peaks of different Zr 3d states. The intensities of high binding energy peaks of Zr 3d<sub>5/2</sub> around 183.7 eV and 182.8 eV were reduced those were assigned for zirconia and high binding energy oxide, respectively. Whereas the peaks at low binding energy around 179.4 eV and 181 eV were gradually dominated as the Ar<sup>+</sup> fluence was increasing in the amounts. Those peaks were assigned for metallic zirconium and low binding energy oxide [30-31]. The values of the peaks were in good agreement with previous data [32]. In Figure 9, the O 1s spectra were composed by two components centered at about 532.9 and 531.1 eV which were attributed to OD<sup>-</sup> and O<sup>2-</sup>, respectively [6, 32-34]. The peak around 532.9 eV was almost disappeared and the peak at 531.1 eV was increased at the initial stage of ion bombardment then decreased after further Ar-ion bombardment.

The peak deconvolution of Zr 3d and O 1s spectra of D<sub>2</sub>O exposed Zircaloy-4 before and after Ar<sup>+</sup> sputtering (Ar<sup>+</sup> fluence ; 12.4 x 10<sup>16</sup> Ar<sup>+</sup>/cm<sup>2</sup>) is depicted in Figure 10 and 11. The Zr 3d peaks (spin orbit splitting is 2.4 eV) at 183.7, 182.8, 181.0 and 179.4 eV were attributed to ZrO<sub>2</sub>, two zirconium oxides and metallic Zr, respectively [5, 30-31]. The oxygen as OD<sup>-</sup>

form was almost removed and the oxygen of  $O^{2-}$  form was considerably reduced after  $Ar^+$  bombardment. The effect of the  $Ar^+$  bombardment was clearly observed as we can in Figure 8~11.  $Ar^+$  bombardment caused a decrease of the oxygen on the surface of Zircaloy-4 and therefore led to change the oxidation state of the zirconium from zirconia to metallic zirconium.

The peak intensities of the different oxidation states of zirconium as a function of the  $Ar^+$  fluence have been depicted in Figure 12. At the initial stage of  $Ar^+$  bombardment, the O 1s intensity of surface oxygen form was increased then gradually decreased with further  $Ar^+$  bombardment (Figure 12(a)). This phenomenon caused sudden increase of zirconium oxides then decrease as we can see in Figure 12(a). Up to around  $5 \times 10^{16} Ar^+/cm^2$ , surface oxygen was depopulated at a certain level then the ratios of the peaks were stayed constant level. This study showed that  $Ar^+$  bombardment was limited to recover metallic zirconium from  $D_2O$  dosed Zircaloy-4.

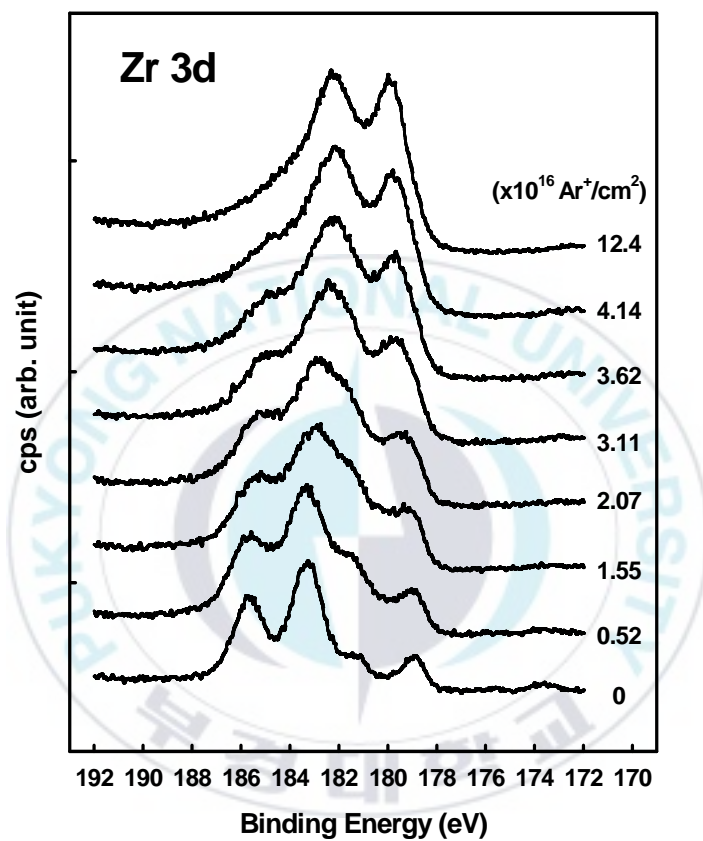


Figure 8. XP spectra of the Zr 3d of D<sub>2</sub>O exposed Zircaloy-4 surfaces after different Ar<sup>+</sup> fluences.

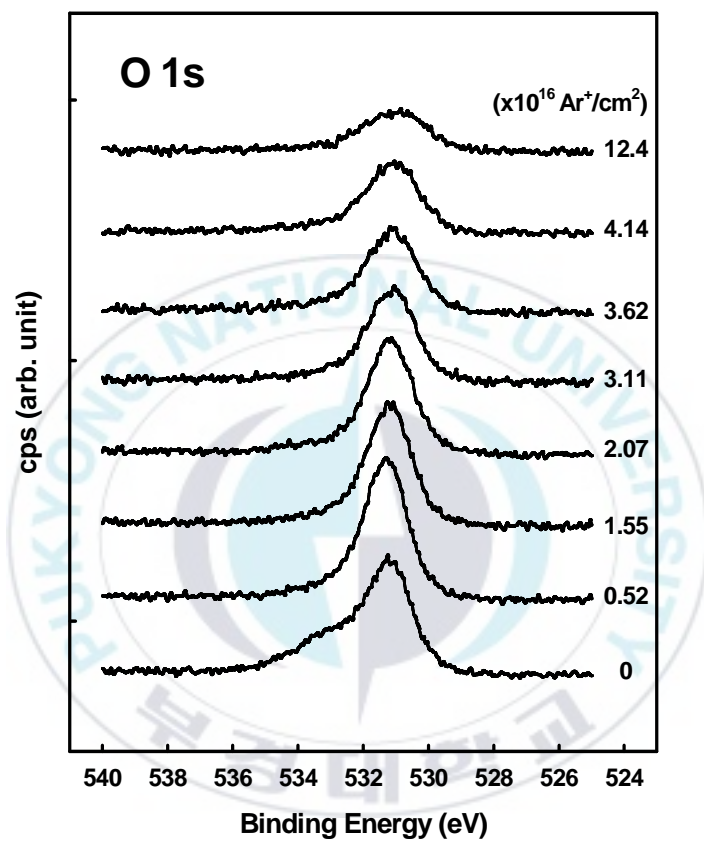


Figure 9. XP spectra of the O 1s of D<sub>2</sub>O exposed Zircaloy-4 surfaces after different Ar<sup>+</sup> fluences.

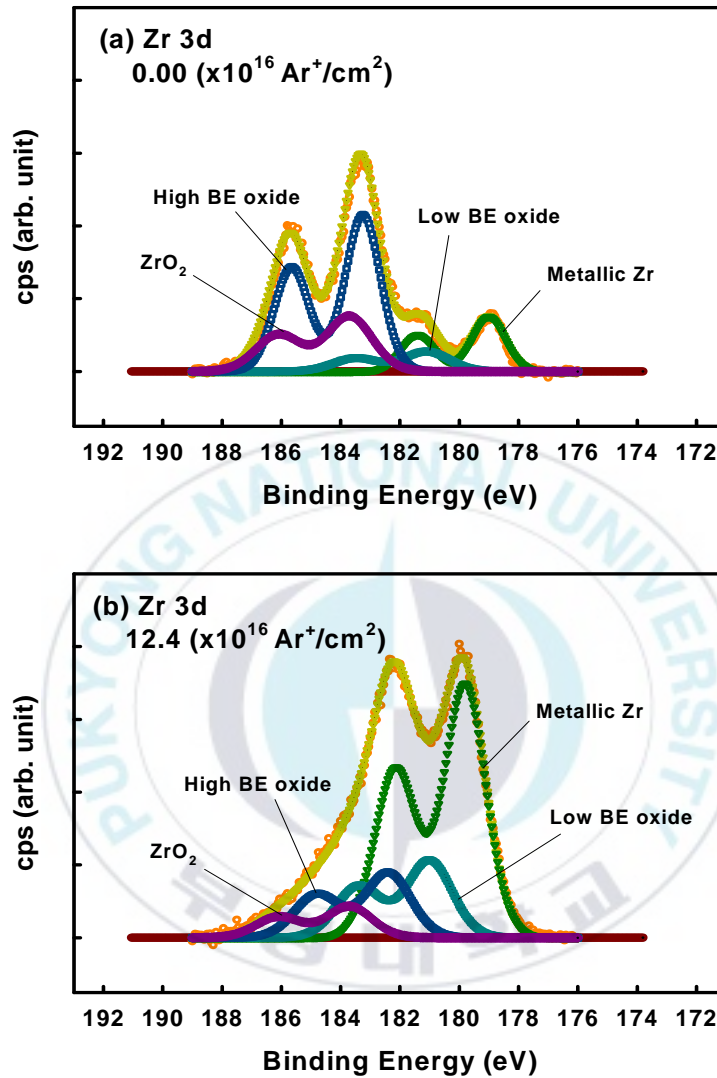


Figure 10. Deconvolution of measured Zr 3d spectra of the D<sub>2</sub>O exposed Zircaloy-4 after different Ar<sup>+</sup> fluences (a) Zr 3d ;  $0.00 \times 10^{16}$  Ar<sup>+</sup>/cm<sup>2</sup> and (b) Zr 3d ;  $12.4 \times 10^{16}$  Ar<sup>+</sup>/cm<sup>2</sup>.

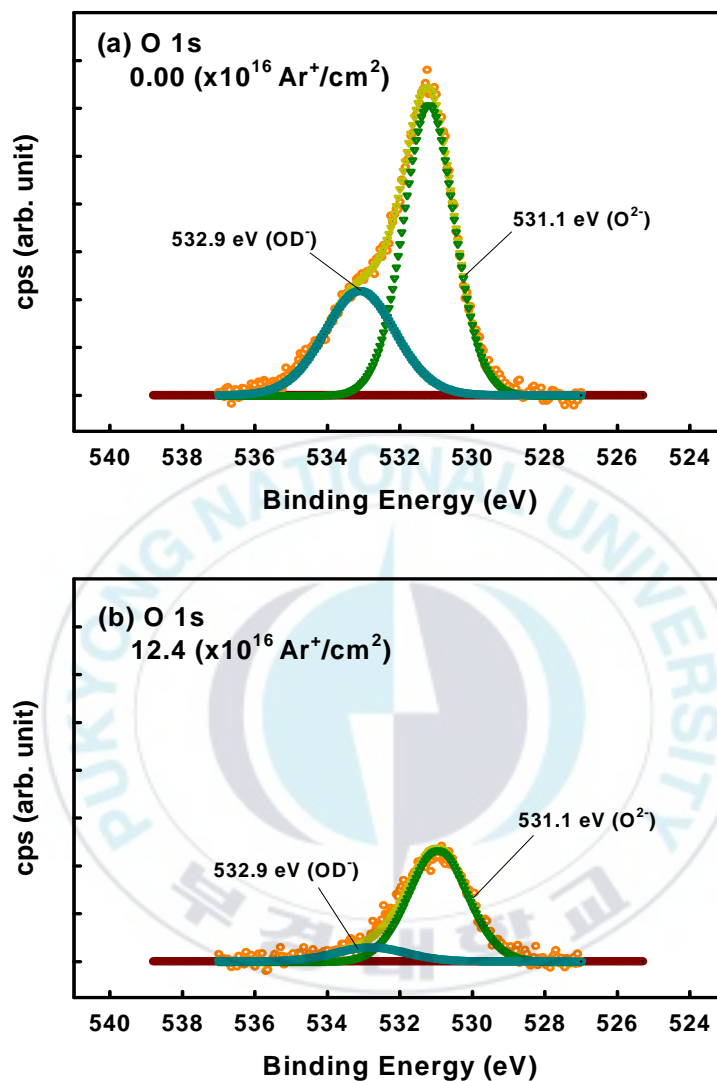


Figure 11. Deconvolution of measured O 1s spectra of the D<sub>2</sub>O exposed Zircaloy-4 after different Ar<sup>+</sup> fluences (a) O 1s ;  $0.00 \times 10^{16} \text{ Ar}^+/\text{cm}^2$  and (b) O 1s ;  $12.4 \times 10^{16} \text{ Ar}^+/\text{cm}^2$ .

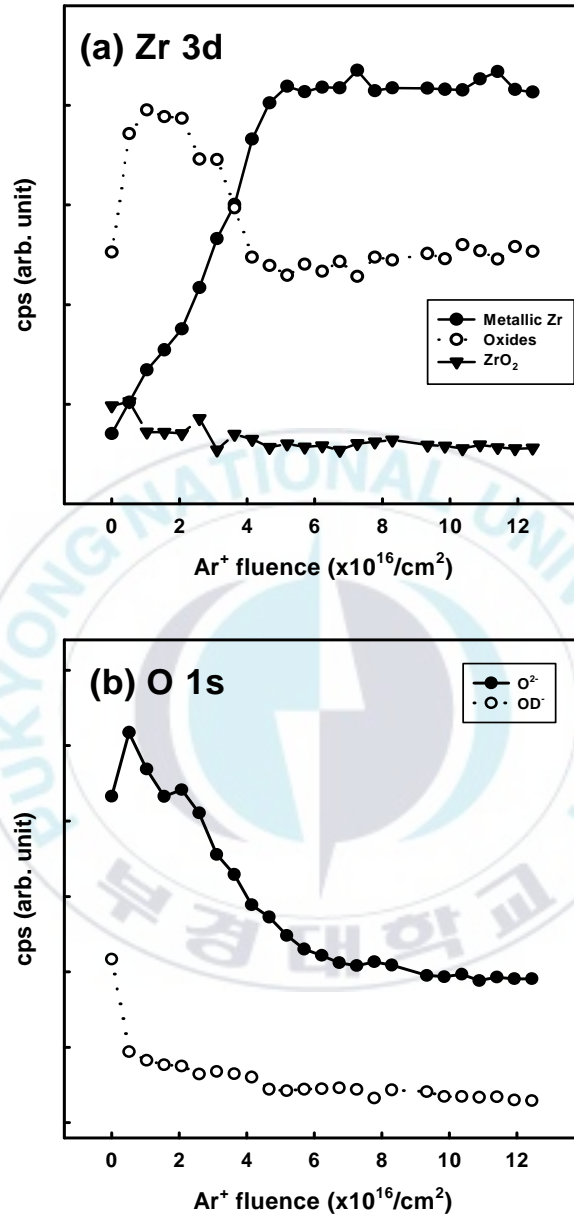


Figure 12. The relative ratios of the Zr 3d (a) and O 1s (b) peaks of the surface of D<sub>2</sub>O exposed Zircaloy-4 as a function of the Ar<sup>+</sup> fluence.

### 3-2. The effect of annealing by using XPS

Figure 13 and 14 represent the evolution of the XP spectra in the Zr 3d and O 1s region of D<sub>2</sub>O dosed Zircaloy-4 after stepwise thermal treatment. The Zr 3d and O 1s XP spectra were composed of several peaks which were ZrO<sub>2</sub> (183.7 eV), two zirconium oxides (182.6 and 180.9 eV) and metallic Zr (179.3 eV) as shown in Figure 9 and 12. Zr 3d XP spectra are stacked up by the annealing temperature in Figure 13. Decrease of the Zr 3d peak intensities at 183.7 and 182.6 eV, which was intense at room temperature, was observed with increasing the annealing temperature and almost vanished at 913 K. While the peak around 179.3 eV was increased at higher temperature and dominated at 913 K. In the Figure 14, the peak shape was changed by annealing temperature. At the highest temperature, the O 1s peak was almost disappeared. We analyzed the peak shape change by deconvolution process. The deconvoluted peaks at the different annealing temperatures are shown in Figure 15 and 16. Up to 787 K, the O 1s peak of O<sup>2-</sup> around 530.9 eV is dominated because the bulk oxygen diffused out to the subsurface region. After that, surface oxygen was depopulated as D<sub>2</sub>O desorption. After 787 K, the O 1s intensity was decreased dramatically. This caused the decrease of zirconium oxide and increase of metallic zirconium.

Figure 17 shows the integrated areas of detailed Zr 3d and O 1s in different chemical environments by the annealing temperature. Annealing of D<sub>2</sub>O dosed Zircaloy-4 surface results in depopulation of oxygen at the surface. This caused conversion of zirconium oxides to metallic zirconium.

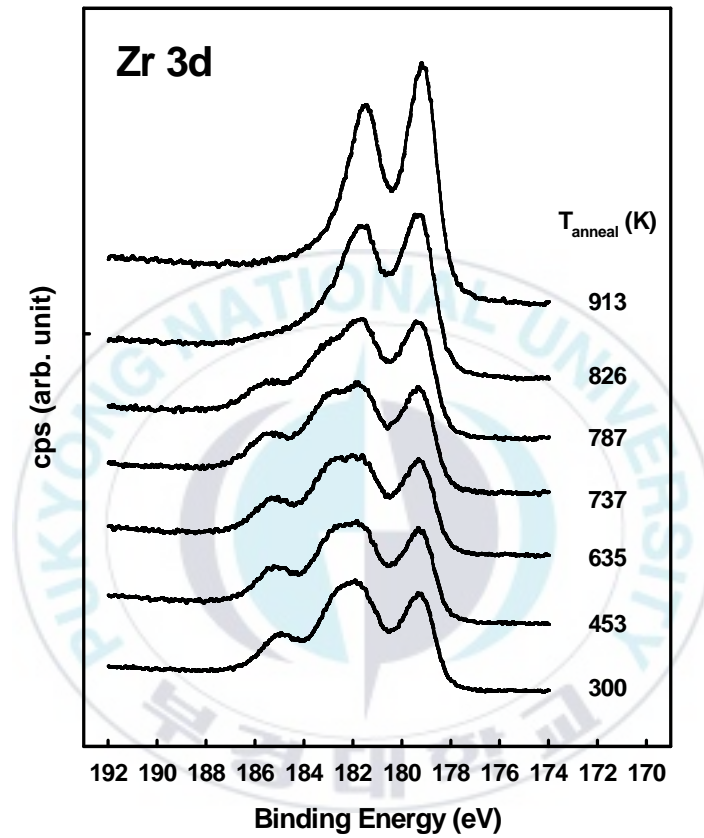


Figure 13. XP spectra of the Zr 3d of D<sub>2</sub>O exposed Zircaloy-4 after stepwise annealing process.

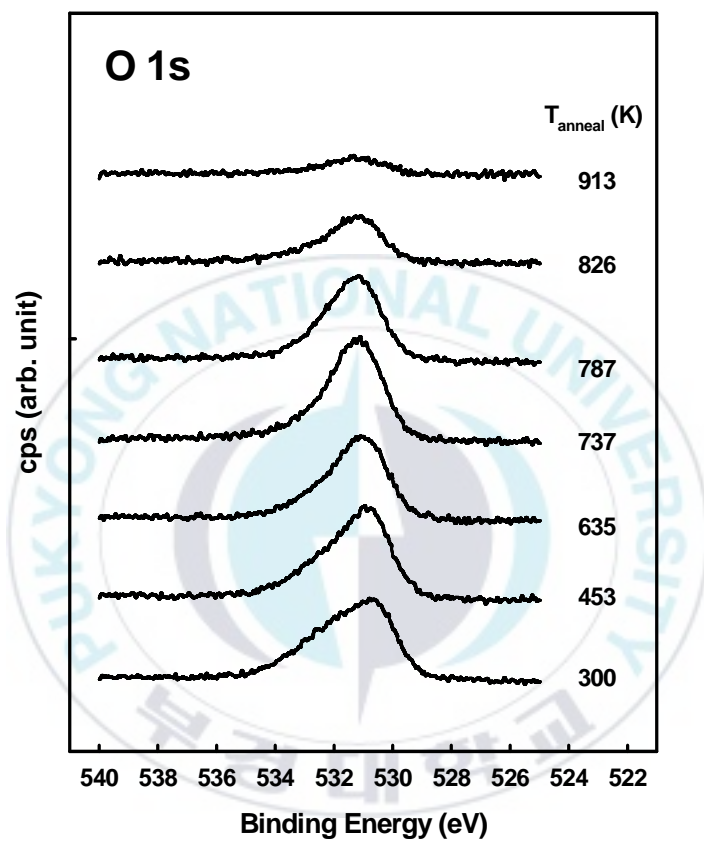


Figure 14. XP spectra of the O 1s of D<sub>2</sub>O exposed Zircaloy-4 after stepwise annealing process.

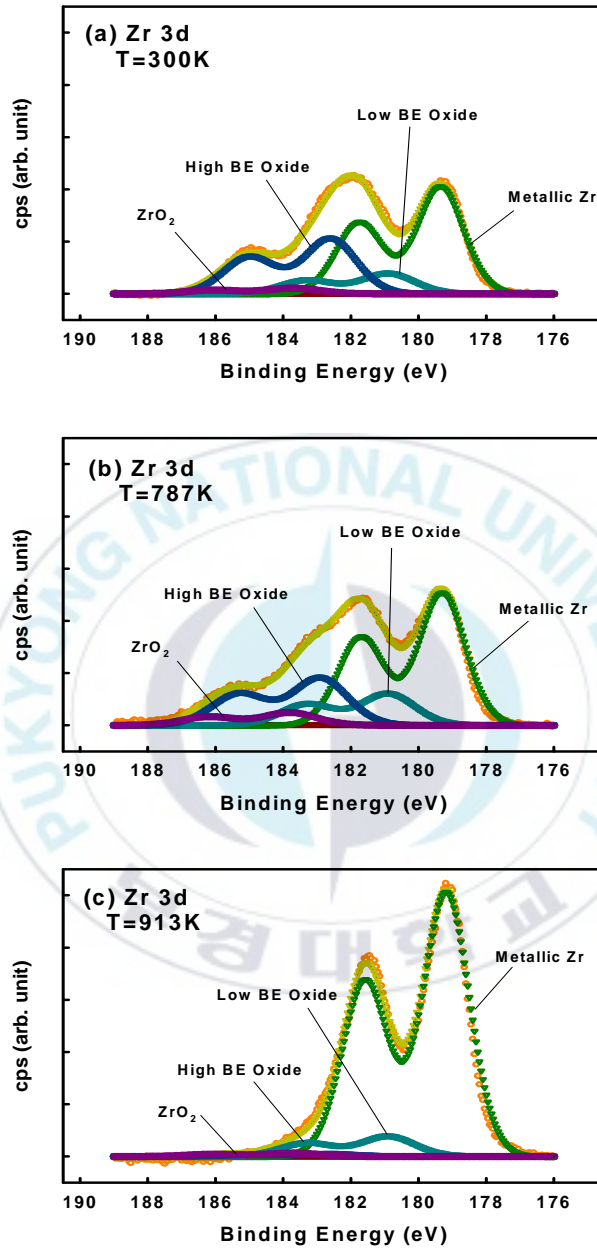


Figure 15. Deconvolution of measured Zr 3d spectra of D<sub>2</sub>O exposed Zircaloy-4 after thermal treatment (a) Zr 3d ; 300 K (b) Zr 3d ; 787 K and (c) Zr 3d ; 913 K.

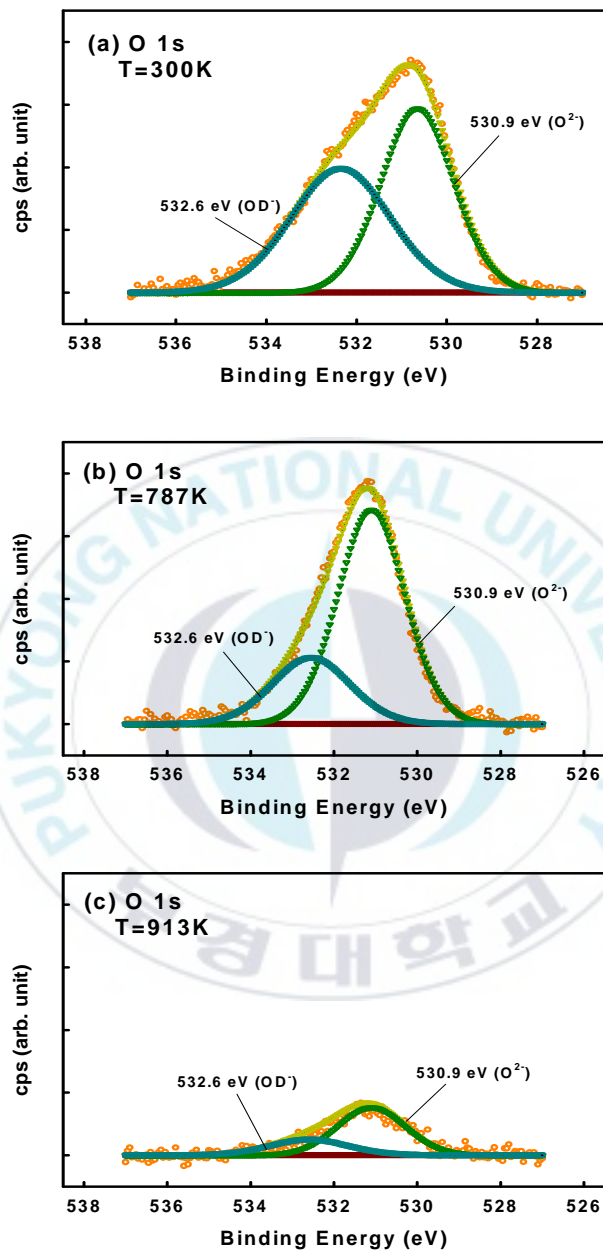


Figure 16. Deconvolution of measured O 1s spectra of D<sub>2</sub>O exposed Zircaloy-4 after thermal treatment (a) O 1s ; 300 K (b) O 1s ; 787 K and (c) O 1s ; 913 K.

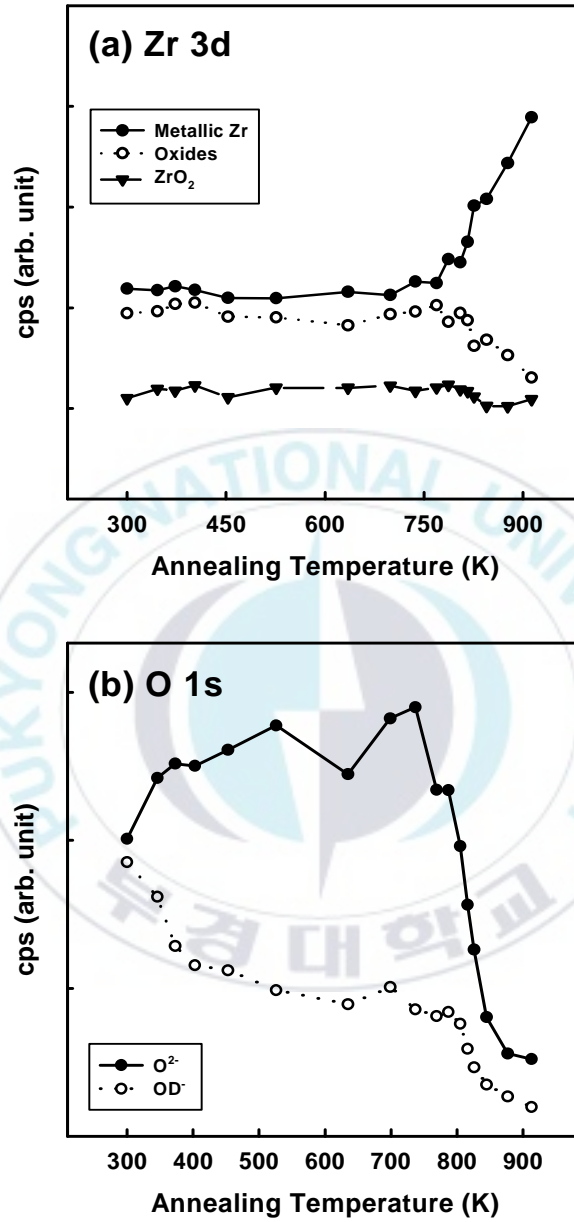


Figure 17. The relative ratios of the Zr 3d (a) and O 1s (b) peaks of the surface of D<sub>2</sub>O exposed Zircaloy-4 as a function of annealing temperature.

### 3-3. The UPS results after Ar<sup>+</sup> sputtering

Due to the lower kinetic energy of the electrons excited from the valence band, UPS has a higher surface sensitivity than XPS [35]. The changes of the valence band structures of D<sub>2</sub>O exposed Zircaloy-4 after stepwise Ar-ion sputtering was studied by means of UPS. The UP spectra were obtained by using He I as the exciting source are shown in Figure 18. The substrate valence band was dominated mainly by the O 2p and Zr 4d orbitals extending from approximately 5 to 16 eV of kinetic energy as shown in Figure 18(a). The window of valence band spectra observed in this study little bit wider than the result of valence band experiment by Sanz et.al. [36]. The valence spectrum of the D<sub>2</sub>O exposed Zircaloy-4 exhibited a dominant peak at around 13 eV which could be assigned to surface ZrO<sub>2</sub> and was attributed to emission from O 2p states interacting with the d-bands of zirconium (bottom line in Figure 18(a)) [35, 37]. The shoulder centered at about 9 eV could be correlated with surface OH which was commonly present on untreated metal surfaces [37]. No Fermi edge was observed in the initial state of Ar<sup>+</sup> sputtering as we can see in Figure 18(a). After stepwise Ar<sup>+</sup> sputtering process, however, there were significant changes of the valence band spectrum, such as the dominant peak at around 13 eV and the shoulder peak at around 9 eV were decreased and the Fermi level was emerged as shown in Figure 18(b). The decrease of the oxygen on the surface of Zircaloy-4 by Ar<sup>+</sup> sputtering led to suppress the dominant peak (ZrO<sub>2</sub>, ~13 eV) and the peak at around 9 eV as surface hydroxide, but develop a new peak of the metallic Zr

4d state (20.5 ~ 21.0 eV) at the Fermi level.

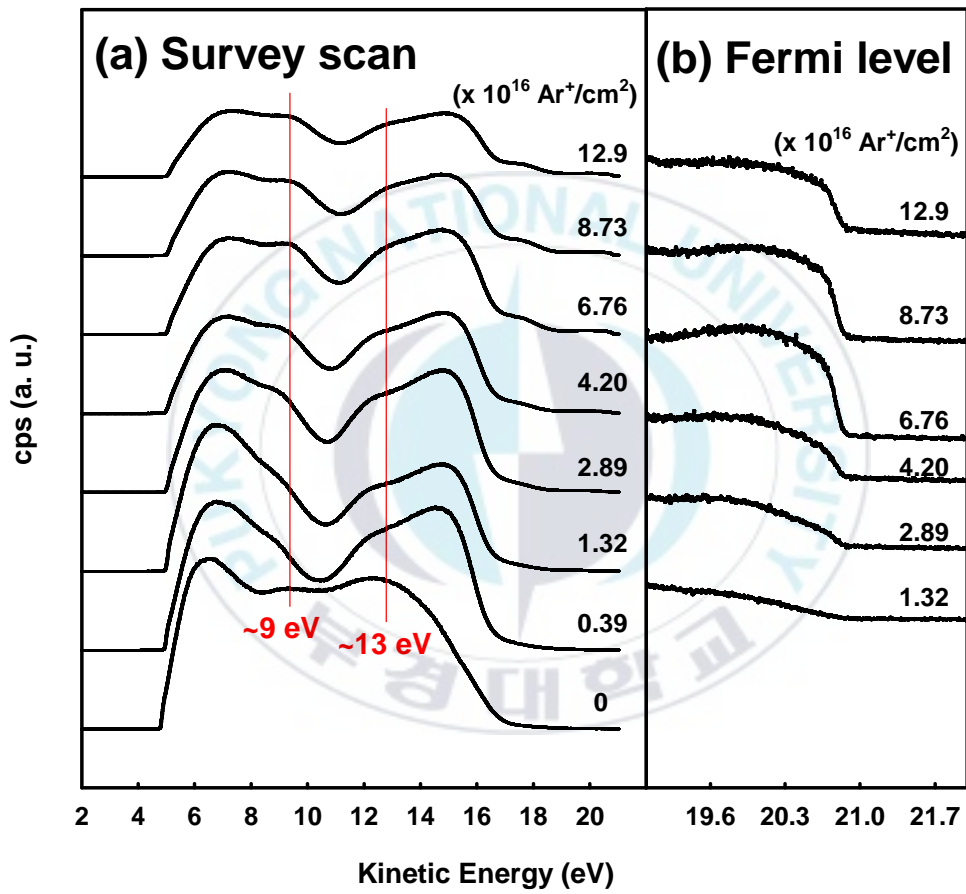


Figure 18. UP spectra of D<sub>2</sub>O exposed Zircaloy-4 after Ar-ion sputtering (a) survey scan and (b) high resolution UP spectra near Fermi level.

## IV. CONCLUSION

New ultra-high vacuum (UHV) system which was designed and constructed for the studies of Zircaloy-4 surface chemistry included a quadruple mass spectrometer (QMS), Auger electron spectroscopy (AES), low-energy electron diffraction (LEED), an argon ion gun for sample cleaning and was housed a gas handling system for temperature programmed desorption (TPD).

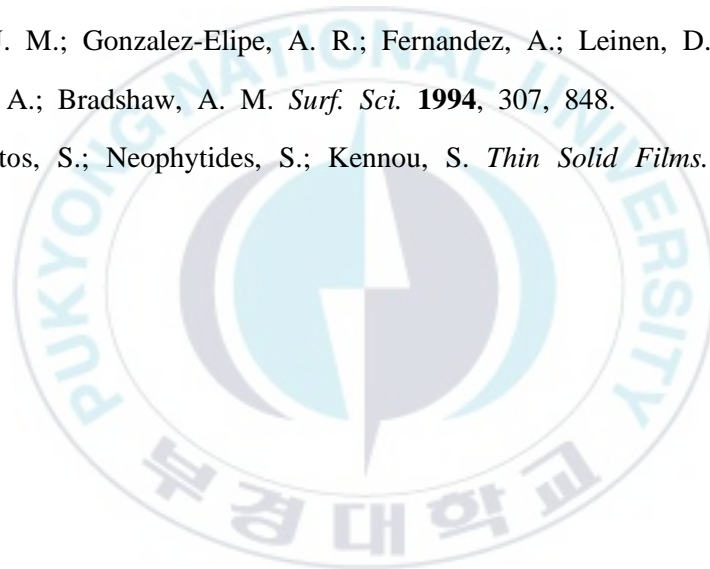
We observed the surface chemistry of D<sub>2</sub>O exposed Zircaloy-4 by Ar-ion sputtering and annealing. In the XPS study, Ar-ion bombardment caused decrease of the oxygen on the surface region of Zircaloy-4 and therefore leads to change the oxidation states of the zirconium from oxide to metallic form. In addition, oxidation states of zirconium were changed to lower oxidation states of zirconium due to depopulated oxygen on the surface region by annealing. Up to about 787 K, the bulk oxygen diffused out to the subsurface region and after this temperature, the oxygen on the surface of Zircaloy-4 was depopulated. UPS study showed that the valence spectrum of the D<sub>2</sub>O exposed Zircaloy-4 exhibited a dominant peak at around 13 eV and no clear Fermi edge was detected. After stepwise Ar<sup>+</sup> sputtering processes, the decrease of the oxygen on the surface of Zircaloy-4 led to suppress the dominant peak at around 13 eV, the peak at around 9 eV and develop the new peak of the metallic Zr 4d state (20.5 ~ 21.0 eV) at the Fermi level.

## V. REFERENCES

- [1] Smith, G. C. *Surface Analysis by Electron Spectroscopy*. **1994**, p 3.
- [2] *XPS Multiulab 2000 System Manual*, (a) *Sample Preparation and Types of Experiment*. p 22. (b) *Optional Sources used on the Multilab 2000*. p 25.
- [3] McCash, E. M. *Surface Chemistry*. **2001**, p 81.
- [4] Childs, K. D. ; Carlson, B. A. ; Lavanier, L. A. ; Moulder, J. F. *Handbook of Auger Electron Spectroscopy*. **1995**, p 2.
- [5] Christmann, K. *Introduction to Surface Physical Chemistry*. **1991**, p 139.
- [6] Wan, Q.; Bai, X.; Zhang. X. *Mater. Res. Bull.* **2006**, 41, 387.
- [7] Kim, W.; Jung, K. S.; Choi, B. H.; Kwon, H. S.; Lee, S. J.; Han, J. G.; Guseva, M. I.; Atamanov, M. V. *Surf. Coat. Technol.* **1995**, 76, 595.
- [8] Chen, X. W.; Bai, X. D.; Deng, P. Y.; Peng, D. Q.; Chen, B. S. *Nucl. Instr. and Meth. B.* **2003**, 211, 512.
- [9] Liu, X.; Bai, X.; Zhou, C.; Wei, L. *Surf. Coat. Technol.* **2004**, 182, 138.
- [10] Bai, X. D.; Wang, S. G.; Xu, J.; Bao, J.; Chen, H. M.; Fan, Y. D. *J. Nucl. Mater.* **1998**, 254, 266.
- [11] Li, J.; Bai, X.; Zhang, D.; Li, H. *Appl. Surf. Sci.* **2006**, 252, 7436.
- [12] Stojilovic, N.; Ramsier, R. D. *J. Nucl. Mater.* **2006**, 350,163.
- [13] Berger, P.; El Tahhann, R.; Moulin, G.; Viennot, M. *Nucl. Instr. and Meth. B.* **2003**, 210, 519.
- [14] Meyer, G.; Kobrinsky, M.; Abriata, J. P.; Bolcich, J. C. *J. Nucl. Mater.* **1996**, 229, 48.
- [15] Gómez, M. P.; Domizzi, G.; López Pumarega, M. I.; Ruzzante, J. E. *J. Nucl. Mater.* **2006**, 353, 167.

- [16] Kim, S. J.; Kim, K. H.; Baek, J. H.; Choi, B. K.; Jeong, Y. H.; Jung, Y. H. *J. Nucl. Mater.* **1998**, 256, 114.
- [17] Fernández, G. E.; Meyer, G., Peretti, H. A. *J. Alloys & Compd.* **2002**, 330, 483.
- [18] Stojilovic, N.; Ramsier, R. D. *Appl. Surf. Sci.* **2006**, 252, 5839.
- [19] Park, K. H.; Cho, Y. C.; Kim, Y. G. *J. Nucl. Mater.* **1999**, 270,154.
- [20] Stojilovic, N.; Ramsier, R. D. *Appl. Surf. Sci.* **2006**, 252, 5839.
- [21] Hong, H. S.; Moon, J. S.; Kim, S. J.; Lee, K. S. *J. Nucl. Mater.* **2001**, 297, 113.
- [22] Bai, X.; Xu, J.; He, F.; Fan, Y. *Nucl. Instr. and Meth. B.* **2000**, 160, 49.
- [23] Stojilovic, N.; Bender, E. T.; Ramsier, R. D. *J. Nucl. Mater.* **2006**, 348, 79.
- [24] Li, B.; Griffiths, K.; Zhang, C. -S.; Norton, P. R. *Surf. Sci.* **1997**, 370, 97.
- [25] Kang, Y. C.; Ramsier, R. D. *Surf. Sci.* **2002**, 519, 229.
- [26] Takagi, I.; Hashizumi, M.; Yamagami, A.; Maehara, K.; Higashi, K. *J. Nucl. Mater.* **1997**, 248, 306.
- [27] Gobrecht, K.; Gutmiedl, E.; Scheuer, A. *Phy. B.* **2002**, 311, 148.
- [28] Charquet, D.; Hahn, R.; Ortlieb, E.; Gros, J. P.; Wadier, J. F. *Zirconium in the Nuclear Industry, San Diego.* **1989**, STP 1023, p. 405.
- [29] Kwon, J. H.; Youn, S. W. ; Kang, Y. C. *Bull. Koeran Chem. Soc.* **2006**, 27, 11.
- [30] Lyapin, A.; Jeurgens, L. P. H.; Mittemeijer, E. J. *Acta. Mater.* **2005**, 53, 2925.

- [31] Lyapin, A.; Jeurgens, L. P. H.; Graat, P. C. J.; Mittemeijer, E. J. *J. Appl. Phys.* **2004**, 96, 12.
- [32] Roustila, A.; Chêne, J.; Séverac, C. *J. Alloys & Compd.* **2003**, 356, 330.
- [33] Morant, C.; Sanz, J. M.; Galán, L. *Phys. Rev. B.* **1992**, 45, 3.
- [34] Wiame, H.; Centeno, M. A.; Picard, S.; Bastians, P.; Grange, P. *J. Eur. Ceram. Soc.* **1998**, 18, 1293.
- [35] Song, Z.; Bao, X.; Wild, U.; Muhler, M.; Ertl, G. *Appl. Surf. Sci.* **1998**, 134, 31.
- [36] Sanz, J. M.; Gonzalez-Elipé, A. R.; Fernandez, A.; Leinen, D.; Galan, L.; Stampfl, A.; Bradshaw, A. M. *Surf. Sci.* **1994**, 307, 848.
- [37] Zafeiratos, S.; Neophytides, S.; Kennou, S. *Thin Solid Films.* **2001**, 386, 53.



## VI. APPENDIX

### PROCEDURE FOR ULTRAVIOLET PHOTOELECTRON SPECTROSCOPY

#### Process

##### Make sure cleanness of He gas line.

- 1) Turn on Roughing Pump (RP) for UPS (but normally "on").  
Cleaning the He gas line (if you need).
    - a. Close the V11, V12 (black round valves near UV lamp), V1 (Main Gate Valve) and V3 (matal angle valve at differential line).
    - b. Open He regulator till 0.5~1 PSI as VX (Red stop valve at Ar gas line) is closed.
    - c. Close the He regulator and open VX then open V18 (He gas inlet).
    - d. Close VX then open V19 (roughing line) slowly for He venting as watching pirani gauge in the pressure gauge controller.  
(V18 and V19 are on the right side of the bench system).
- \* Repeat c and d as you need (4-5 times).

After He gas line is cleaned,

- 2) Open VX, open V18, close V19.
- 3) Open V11 slowly.

4) Open V12 slowly (pressure increased little bit).

Maximum pressure change should be less than "one" order by ion gauge.

5) Set the current knob on UPS controller maximum (clockwise).

6) Push the power button on UV unit.

(multimeter(kV) value should reach almost the end of the meter scale).

7) Open V13 (leak valve) slowly to admit He.

8) When the color of the UV lamp changes to white pink (about  $5 \times 10^{-8} \sim 5 \times 10^{-7}$  mbar), close V13 slowly to reduce the pressure (about  $7 \times 10^{-8}$  mbar) but the lamp must be turned on.

## Program

1) Click the user set up page - Lens Mode - Select "UPS".

2) Start Avantage.

3) Manual source - Selected Gun Mode - Select "He I".

4) Experiment - "Manual point" - "Scan".

Energy scale - "Kinetic".

Mode - "CAE".

Energy Ranges - "UPS".

Lens mode - "UPS".

Start E - "21.2" eV.

End E - "0" eV.

Energy step size - "0.05" eV.

Pass energy - "2" eV.

Dwell time - "50" ms.

Click "Apply".

### **Turn off UPS**

- 1) Turn off UPS power on the controller
- 2) Close VX and V13
- 3) After 20-30 min, close V11 and V12.



## KOREAN ABSTRACT

새로운 UHV 시스템 제작과 D<sub>2</sub>O/Zircaloy-4의 표면 화학

오 경 선

부경대학교 대학원 화학과

요 약

Chapter 1에서 초고진공 (UHV) 시스템은 지르칼로이-4 (Zircaloy-4) 의 표면 화학 연구를 위해 디자인 되고 제작되었다. 초고진공은 roughing pump (RP), turbomolecular pump (TMP), titanium sublimation pump (TSP) 그리고 두개의 ion pumps (IP)에 의해 만들어졌다. 초고진공 챔버는 Auger electron spectroscopy (AES), low-energy electron diffraction (LEED)가 장착 되어 있고 temperature programed desorption (TPD) 실험을 위해 quadruple mass spectrometer (QMS)가 부착되었으며 gas handling system이 설치되었다. 또한 샘플 cleaning을 위해 argon ion gun이 부착되어 있다.

Chapter 2에서는 중수(D<sub>2</sub>O)를 흡착시킨 지르칼로이-4(Zircaloy-4)를 아르곤 이온 스퍼터링(Ar-ion bombardment)과 가열(annealing)을 한 후에 그 표면현상을 XPS (X-ray photoelectron spectroscopy)와 UPS (Ultraviolet photoelectron spectroscopy)로 연구했다. XPS 연구 결과에서, 아르곤 이온 스퍼터링과 열에 의한 영향이 분명하게 관찰 되었다. 아르곤 스퍼터링은 지르칼로이-4의 표면 위에 있는 산소를 점점 고갈시켰으며 열 또한 표면의 산소를 제거하는 원인이 되었다. 그것은 지르코늄의 산화상태가 낮은 상태로의 변화를 이끌었다. UPS 연구는 아르곤 이온 스퍼터링 후에 산소가 사라지면서 약 13 eV 부근의 주된 피크와 약 9 eV의 피크 감소되고 페르미 레벨에서 metallic Zr 4d 상태의 새로운 피크의 발전을 이끈 것을 보여준다.

## ACKNOWLEDGMENT

*I would like to express my gratitude to special people.*

*First of all, I deeply thank my supervisor, Prof. Yong-Cheol Kang, for his teaching, support, guidance and kindness throughout the two years. It was kind of difficult time for him and me at the beginning due to some problems with UHV system in our laboratory. However, I'm really glad that the construction of UHV system was done and the TPD experiment is being conducted now. I believe that everything is going to be okay and my juniors, Ju-Yun Park, Se Won Jung, Mi Sun Chun are doing well.*

*I sincerely thank Professor, Dong J Lee and Don Kim, for their valuable time and advice about my thesis.*

*I would like to thank all professors in chemistry department and all of my lab members, especially, Ji Hye Kwon, Hye Yoon Jung, Sang Yong Han and Seon Kyong Kim. They really helped me in many ways. I can't forget my interesting life with them in our lab.*

*I also thank my special friends, Su Jin Shin, Jeong Im Eom, Cheon Ja Mun, Jeong Im Kwon, Im Sun Jung, Mi Kyung Kim, Soo Jung Park and Sang Joe Kim. Thanks to them, I am always happy.*

*Lastly I really appreciate my family and my lover' helps, support, endless love and encouragement.*

*August 2007*

*Kyung-Sun Oh*